An Octanuclear Complex Containing the {Fe 3 O} 7+ Metal Core: Structural, Magnetic, Mössbauer, and Electron Paramagnetic Resonance Studies

5 AUTHORS, INCLUDING:

Athanassios K. Boudalis
Florida International University
69 PUBLICATIONS **1,473** CITATIONS

SEE PROFILE

Yiannis Sanakis
National Center for Scientific Research Demo…
134 PUBLICATIONS **3,477** CITATIONS

SEE PROFILE

Inorganic Chemistry

Article

An Octanuclear Complex Containing the $\{Fe_3O\}^{7+}$ Metal Core: Structural, Magnetic, Mössbauer, and Electron Paramagnetic Resonance Studies[#]

Athanassios K. Boudalis,*,†,‡ Yiannis Sanakis,*,‡ Françoise Dahan,† Michael Hendrich,§ and Jean-Pierre Tuchagues†

Laboratoire de Chimie de Coordination du CNRS, UPR 8241, 205 route de Narbonne, 31077 Toulouse Cedex 04, France, Institute of Materials Science, NCSR "Demokritos", 15310 Aghia Paraskevi Attikis, Greece, and Department of Chemistry, Carnegie Mellon University, 4400 Fifth Avenue, Pittsburgh, Pennsylvania 15213

A new asymmetrically coordinated bis-trinuclear iron(III) cluster containing a $\{Fe_3O\}^{7+}$ core has been synthesized and structurally, magnetically, and spectroscopically characterized. $[Fe_6Na_2O_2(O_2CPh)_{10}(pic)_4(EtOH)_4(H_2O)_2](ClO_4)_2 \cdot$ 2EtOH (**1**·2EtOH) crystallizes in the $P\bar{1}$ space group and consists of two symmetry-related $\{Fe_3O\}^{7+}$ subunits linked by two Na^+ cations. Inside each $\{Fe_3O\}^{7+}$ subunit, the iron(III) ions are antiferromagnetically coupled, and their magnetic exchange is best described by an isosceles triangle model with two equal (J) and one different (J') coupling constants. On the basis of the $H = -2\Sigma J_{ij}S_iS_j$ spin Hamiltonian formalism, the two best fits to the data yield solutions $J = -27.4$ cm^{-1}, $J' = -20.9$ cm^{-1} and $J = -22.7$ cm^{-1}, $J' = -31.6$ cm^{-1}. The ground state of the cluster is $S = 1/2$. X-band electron paramagnetic resonance (EPR) spectroscopy at liquid-helium temperature reveals a signal comprising a sharp peak at $g \sim 2$ and a broad tail at higher magnetic fields consistent with the $S = 1/2$ character of the ground state. Variable-temperature zero-field and magnetically perturbed Mössbauer spectra at liquid-helium temperatures are consistent with three antiferromagnetically coupled high-spin ferric ions in agreement with the magnetic susceptibility and EPR results. The EPR and Mössbauer spectra are interpreted by assuming the presence of an antisymmetric exchange interaction with $|\mathbf{d}| \sim 2$–4 cm^{-1} and a distribution of exchange constants J_{ij}.

Introduction

The magnetic properties of trinuclear carboxylate complexes of the type $[M_3O(O_2CR)_6L_3]^{0/+}$, where M is a first-row transition metal and L is a terminal ligand, have been the subject of numerous studies over the past decades.[1] These clusters were among the first polynuclear compounds for which the isotropic Heisenberg−Dirac−van Vleck Hamiltonian (HDvV; eq 1) was proposed for interpreting their magnetic properties, and it was analytically solved and applied in the cases $J_{12} = J_{13} = J_{23} = J$ (equilateral model) and $J_{12} = J_{13} = J$ and $J_{23} = J'$ (isosceles model).[2]

$$\hat{H}_{\text{HDvV}} = -2(J_{12}\hat{S}_1\hat{S}_2 + J_{13}\hat{S}_1\hat{S}_3 + J_{23}\hat{S}_2\hat{S}_3) \qquad (1)$$

Most trinuclear carboxylate complexes studied to date exhibit symmetric coordination environments around the three metal centers; on the basis of ambient-temperature crystal structure determinations, the metal ions form an equilateral triangle. This equilateral triangle configuration suggests that the magnetic properties should be described assuming three equal exchange parameters J_{ij}. However, it

* To whom correspondence should be addressed. E-mail: tbou@ ims.demokritos.gr (A.K.B.), sanakis@ims.demokritos.gr (Y.S.).
† Laboratoire de Chimie de Coordination du CNRS.
‡ Institute of Materials Science, NCSR "Demokritos".
§ Carnegie Mellon University.

(1) For example, see: (a) Cannon, R. D.; White, R. P. *Prog. Inorg. Chem.* **1988**, *36*, 195. (b) Bond, A. M.; Clark, R. J. H.; Humphrey, D. G.; Panayiotopoulos, P.; Skelton, B. W.; White, A. H. *J. Chem. Soc., Dalton Trans.* **1998**, 1845. (c) Wu, R.; Poyraz, M.; Sowrey, F. E.; Anson, C. E.; Wocadlo, S.; Powell, A. K.; Jayasooriya, U. A.; Cannon, R. D.; Nakamoto, T.; Katada, M.; Sano, H. *Inorg. Chem.* **1998**, *37*, 1913.

(2) In fact, Kambe first applied his spin-coupling approach to interpret the magnetic behavior of basic trinuclear iron carboxylate complexes: Kambe, K. *J. Phys. Soc. Jpn.* **1950**, *5*, 48.

was soon realized that their low-temperature magnetic susceptibility data could not be described assuming three equal exchange constants.

To correctly account for the low-temperature magnetic measurements, it was necessary to assume that at least one of the J_{ij} constants was different. This inequality of J_{ij} lifts the degeneracy of the ground $S = \frac{1}{2}$ states imposed by the equilateral model. The degeneracy lifting of the ground state was later confirmed by inelastic neutron scattering (INS) experiments.[3]

The inequality of the J_{ij} constants has puzzled researchers because this is not expected if one considers the equilateral geometry shown by the ambient-temperature crystal structure. The concept of the "magnetic Jahn−Teller effect" was thus introduced to account for a ground state characterized by isosceles rather than equilateral symmetry.[4]

Magnetic susceptibility measurements provide invaluable information for the determination of the magnitude of the J_{ij} constants. The isotropic H_{HDvV} Hamiltonian (1) is usually employed for analyzing these data, and as we have already discussed, analysis of these measurements revealed the necessity for a symmetry reduction of the triangle configuration. However, magnetic susceptibility measurements are not helpful in determining the influence of other factors such as anisotropic interactions, zero-field splitting (ZFS), etc., in trinuclear complexes. Other experimental techniques have helped to reveal the role of these factors. Electron paramagnetic resonance (EPR) spectroscopy, in the case of M = chromium(III),[5] iron(III),[6] and more recently copper(II),[7] has revealed significant anisotropy for the $S = \frac{1}{2}$ ground state. To account for this anisotropy, eq 1 was augmented with anisotropic terms and especially the antisymmetric exchange (AE) or Dzialoshinsky−Moriya term.[6a,8,9] This term also increases the separation of the two $S = \frac{1}{2}$ ground states, and with regards to magnetic susceptibility, AE has the same effect as the inequality of the J_{ij} constants.[9] Therefore, the combination of various experimental techniques is necessary in order to ascertain quantitatively the contribution of each of the various factors that regulate the magnetic properties of trinuclear complexes.

The properties of trinuclear complexes are of general interest because such complexes are found in the active sites of iron−sulfur proteins[10] or copper enzymes.[11] In the case of $[3Fe−4S]^+$ clusters, a combination of EPR and Mössbauer techniques revealed that apart from AE[12] of importance also is a distribution of the exchange parameters J_{ij} (J strain).[12,13] Some polynuclear transition-metal complexes, referred to as single-molecule magnets (SMMs), exhibit interesting magnetic properties such as stepwise magnetization hysteresis loops due to inherent properties of the individual molecules rather than long-range ordering.[14] The importance of non-Heisenberg interactions in modulating these properties is well-known.[14] To quantitatively account for the contribution of these interactions in the magnetic properties of polynuclear compounds, it is useful to elucidate the behavior of clusters with lower nuclearity and trinuclear complexes are suitable for this task.

Here we report on the synthesis and crystallographic characterization of a complex containing the $\{Fe_3O\}^{7+}$ core. The crystal structure of this complex reveals asymmetry; two of the ferric ions possess a NO_5 chromophore, whereas the environment of the remaining ion consists of six oxygen atoms. Departure from C_3 symmetry is expected to result in different exchange coupling constants between the ferric pairs, affecting thus the magnetic properties of the ground state. Indeed, in some asymmetric trinuclear ferric complexes, the lowering of the symmetry results in a $S = \frac{5}{2}$ ground state.[15,16] The complex under study is shown to possess a ground state with $S = \frac{1}{2}$. Because the exchange coupling constants J_{ij} are different, this complex is a model well suited to examine the effects of the other factors assumed to influence the magnetic properties. To achieve this goal, we have combined various experimental techniques (magnetic susceptibility measurements and EPR and Mössbauer spectroscopy). We provide a set of parameters that quantitatively accounts for all of the observations.

Experimental Section

Materials. All reagents and solvents were of analytical grade and were used as received, except sodium picolinate (Napic), which was prepared by the reaction of an aqueous solution of picolinic acid with $NaHCO_3$ in a 1:1 ratio. The syntheses were carried out under aerobic conditions. ***Warning!*** *Although no such tendency was observed during the current work, perchlorate salts are potentially explosive and should be handled with caution and in small quantities.*

(3) (a) Cannon, R. D.; Jayasooriya, U. A.; Wu, R.; arapKoske, S. K.; Stride, J. A.; Nielsen, O. F.; White, R. P.; Kearley, G. J.; Summerfield, D. *J. Am. Chem. Soc.* **1994**, *116*, 11869. (b) Stride, J. A.; Jayasooriya, U. A.; Eckert, J. *Angew. Chem., Int. Ed.* **1999**, *38*, 116. (c) Sowrey, F. E.; Tilford, C.; Wocadlo, S.; Anson, C. E.; Powell, A. K.; Bennington, S. M.; Montfrooij, W.; Jayasooriya, U. A.; Cannon, R. D. *J. Chem. Soc., Dalton Trans* **2001**, 862.

(4) Murao, T. *Phys. Lett. A* **1974**, *49*, 33.

(5) (a) Yablokov, Y. V.; Gaponenko, V. A.; Ablov, A. V.; Zhkhareva, T. N. *Sov. Phys. Solid State* **1973**, *15*, 251. (b) Nishimura, H.; Date, M. *J. Phys. Soc. Jpn.* **1985**, *54*, 395. (c) Honda, M.; Morita, M.; Date, M. *J. Phys. Soc. Jpn.* **1992**, *61*, 3773. (d) Vlachos, A.; Psycharis, V.; Raptopoulou, C. P.; Lalioti, N.; Sanakis, Y.; Fardis, M.; Karayanni, M.; Papavassiliou, G.; Terzis, A. *Inorg. Chim. Acta* **2004**, *357*, 3162.

(6) (a) Rakitin, Y. V.; Yablokov, Y. V.; Zelentzov, V. V. *J. Magn. Reson.* **1981**, *43*, 288. (b) Caneschi, A.; Cornia, A.; Fabretti, A. C.; Gatteschi, D.; Malavasi, W. *Inorg. Chem.* **1995**, *34*, 4660.

(7) (a) Liu, X. M.; de Miranda, M. P.; McInnes, E. J. L.; Kilner, C. A.; Halcrow, M. A. *Dalton Trans.* **2004**, 59. (b) Yoon, J.; Mirica, L. M.; Stack, D. P.; Solomon, E. I. *J. Am. Chem. Soc.* **2004**, *126*, 12586. (c) Belinsky, M. I. *Inorg. Chem.* **2004**, *43*, 739.

(8) Gaponenko, V. A.; Eremin, M. V.; Yablokov, Y. V. *Sov. Phys. Solid State* **1973**, *909*, 909.

(9) Tsukerblat, B. S.; Belinski, M. I.; Fainzil'berg, V. E. *Sov. Sci. Rev., Sect. B* **1987**, *9*, 337.

(10) Guigliarelli, B.; Bertrand, P. *Adv. Inorg. Chem.* **1999**, *47*, 421.

(11) Lee, S. K.; George, S. D.; Antholine, W. E.; Hedman, B.; Hodgson, K. O.; Solomon, E. I. *J. Am. Chem. Soc.* **2002**, *124*, 6180.

(12) Sanakis, Y.; Macedo, A. L.; Moura, I.; Moura, J. J. G.; Papaefthymiou, V.; Munck, E. *J. Am. Chem. Soc.* **2000**, *122*, 11855.

(13) Krebs, C.; Henshaw, T. F.; Cheek, J.; Huynh, B. H.; Broderick, J. B. *J. Am. Chem. Soc.* **2000**, *122*, 12497.

(14) Gatteschi, D.; Sessoli, R. *Angew. Chem., Int. Ed.* **2003**, *43*, 268.

(15) Bill, E.; Krebs, C.; Winter, M.; Gerdan, M.; Trautwein, A. X.; Florke, U.; Haupt, H. J.; Chaudhuri, P. *Chem.−Eur. J.* **1997**, *3*, 193.

(16) Gorun, S. M.; Papaefthymiou, G. C.; Frankel, R. B.; Lippard, S. J. *J. Am. Chem. Soc.* **1987**, *109*, 4244.

**Synthesis of [Fe₆Na₂O₂(O₂CPh)₁₀(pic)₄(EtOH)₄(H₂O)₂](ClO₄)₂·
2EtOH (1·2EtOH).** Solid Napic (0.348 g, 2.40 mmol) was added
to a stirred solution of Fe(ClO₄)₃·6H₂O (1.109 g, 2.40 mmol) and
NaO₂CPh (0.605 g, 4.20 mmol) in EtOH (25 mL), and the solution
was refluxed. Upon Napic dissolution, the deep-red solution turned
dark red. After ∼15−30 min of refluxing, the solution was hot
filtered and left to cool undisturbed. After ca. 1 day, orange
parallelepiped crystals of **1**·2EtOH had formed. They were collected
by filtration, washed with cold EtOH, and dried in vacuo. The yield
was 0.24 g (∼24%). Analytical data calculated (observed) for
C₁₀₂H₉₄N₄O₄₄Na₂Cl₂Fe₆: C, 48.39 (48.23); H, 3.74 (3.55); N, 2.21,
(2.23); Cl, 2.80 (2.95); Fe, 13.24 (13.02). Selected IR bands (KBr,
cm⁻¹): 3414 (m, b), 3065 (m), 1667 (s), 1621 (s), 1560 (vs), 1554
(vs), 1493 (m), 1476 (w), 1408 (vs, b), 1362 (s), 1293 (m), 1260
(w), 1177 (m), 1093 (s, b), 1070 (s), 1047 (m), 1024 (m), 1002
(w), 938 (w), 865 (m), 841 (w), 818 (w), 763 (m), 720 (s), 697
(m), 675 (m), 622 (s), 483 (s).

Measurements. Microanalyses were performed by the Mi-
croanalytical Laboratory of the Laboratoire de Chimie de Coordina-
tion at Toulouse and at the Service Central de Microanalyses du
CNRS in Vernaison, France, for Fe and Cl. Infrared spectra (4000−
400 cm⁻¹) were recorded as KBr disks on a Perkin-Elmer 16PC
spectrometer.

Mössbauer measurements were recorded on a constant-accelera-
tion conventional spectrometer with a 50-mCi source of ⁵⁷Co (Rh
matrix). The absorber was a powdered sample enclosed in a 20-
mm-diameter, cylindrical, plastic sample holder, the size of which
had been determined to optimize the absorption. Zero-field, variable-
temperature spectra were obtained in the 4.2−300 K range by using
an Oxford MD 306 cryostat, with the thermal scanning being
monitored by an Oxford ITC4 servocontrol device (±0.1 K
accuracy). Isomer shift values (δ) are reported relative to an iron
foil at 293 K. Variable-field/variable-temperature spectra were
obtained by using an Oxford cryostat equipped with a supercon-
ducting magnet with the magnetic field perpendicular to the γ-rays.
The spectra were analyzed by using the program WMOSS (Web
Research, Edina, MN).

Variable-temperature (2−300 K) magnetic susceptibility data
were collected on a powdered microcrystalline solid on a Quantum
Design MPMS SQUID susceptometer under a field of 10 kG. Data
were corrected with standard procedures for the contribution of the
sample holder and diamagnetism of the sample. The magnetic
susceptibility has been computed by exact calculation of the energy
levels associated with the spin Hamiltonian through diagonalization
of the full matrix with a general program for axial symmetry.[17]
Least-squares fittings were accomplished with an adapted version
of the function-minimization program MINUIT.[18] The error factor
R is defined as $R = \sum[(x_{exp} - x_{calc})^2/Nx_{exp}^2]$, where N is the number
of experimental points.

X-band EPR spectra at liquid-helium temperatures were recorded
on a Bruker ER 200D-SRC X-band spectrometer equipped with
an Oxford ESR 9 cryostat, an NMR gaussmeter, and an Anritsu
microwave frequency counter. Q-band EPR spectra were recorded
on an instrument described in ref 19. Simulations of the spectra
were performed by using home-written routines.

X-ray Crystallography. The crystallographic data together with
the refinement details for **1** are summarized in Table 1.

Table 1. Crystallographic Data Collection and Structure Determination

	1·2EtOH
formula	C₁₀₆H₁₀₆Cl₂Fe₆N₄Na₂O₄₆
fw	2623.93
cryst syst	triclinic
space group	$P\bar{1}$ (No. 2)
T, K	160
unit cell dimens	
a, Å	11.4457(11)
b, Å	14.7935(14)
c, Å	18.0086(16)
α, deg	88.843(13)
β, deg	75.571(11)
γ, deg	87.569(13)
V, Å³	2950.3(5)
Z	1
ρ_{calc}, g cm⁻³	1.477
λ, Å	Mo Kα, 0.710 73
μ, mm⁻¹	0.860
R, R_w (all data)^{a,b}	0.0502, 0.0642
R, R_w ($I > 2\sigma(I)$)^{a,b}	0.0368, 0.0623

$^a R = \sum||F_o| - |F_c||/\sum|F_o|.$ $^b R_w = [\sum w(|F_o|^2 - |F_c|^2)^2/\sum w|F_o^2|^2]^{1/2}.$

The selected crystal of **1**·2EtOH (orange prism, 0.45 × 0.30 ×
0.15 mm) was mounted on a Stoe Imaging Plate Diffractometer
System equipped with an Oxford Cryosystems cooler device at 160
K using a graphite monochromator (λ = 0.710 73 Å). The crystal-
to-detector distance was 70 mm (max 2θ value = 52.1°). Data were
collected with a φ oscillation movement (φ = 0.0−249.6°; Δφ =
1.3°). Numerical absorption corrections were applied (T_max =
0.6238; T_min = 0.3801).

The structure was solved by direct methods using SHELXS-
97[20] and refined by full-matrix least-squares on $F_o{}^2$ using SHELXL-
97[21] with anisotropic displacement parameters for all non-hydrogen
atoms. All H atoms were introduced in calculations using the riding
model with isotropic thermal parameters 1.1 times higher than those
of the riding atom, except those bonded to O16 (water molecule)
and those bonded to the oxygen atoms O17 and O18 of the ethanol
molecules, which were allowed to vary.

Scattering factors were taken from the literature.[22] The molecular
plots were obtained using the ORTEP32 program.[23]

Results and Discussion

Synthesis. It was believed that picolinate anions would
exhibit a chelating coordination mode, as was previously
observed for iron(III),[24] vanadium(III),[25] and manganese(III)[26]
carboxylate clusters. However, the bridging coordination
mode cannot be a priori excluded, which is very interesting
from a synthetic point of view, to assemble larger polyme-
tallic arrays. Reaction of Fe(ClO₄)₃·6H₂O, NaO₂CPh, and
Napic in a 1:1.75:1 ratio in boiling EtOH led to a dark-red

(17) Clemente-Juan, J.-M.; Mackiewicz, C.; Verelst, M.; Dahan, F.;
Bousseksou, A.; Sanakis, Y.; Tuchagues, J.-P. *Inorg. Chem.* **2002**,
41, 1478.
(18) James, F.; Roos, M. *MINUIT Program*, a System for Function
Minimization and Analysis of the Parameters Errors and Correlations.
Comput. Phys. Commun. **1975**, *10*, 345.
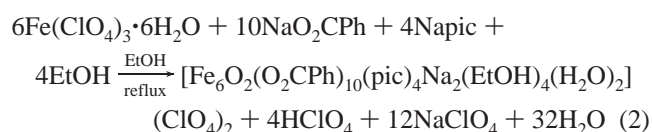(19) Petasis, D.; Hendrich, M. P. *J. Magn. Reson.* **1999**, *136*, 200.
(20) Sheldrick, G. M. *SHELXS-97, Program for Crystal Structure Solution*;
University of Göttingen: Göttingen, Germany, 1997.
(21) Sheldrick, G. M. *SHELXL-97, Program for the Refinement of Crystal
Structures from Diffraction Data*; University of Göttingen: Göttingen,
Germany, 1997.
(22) *International Tables for Crystallography*; Kluwer Academic Publish-
ers: Dordrecht, The Netherlands, 1992; Vol. C, Tables 4.2.6.8 and
6.1.1.4.
(23) ORTEP32 for Windows: Farrugia, L. J. *J. Appl. Crystallogr.* **1997**,
30, 565.
(24) Wemple, M. W.; Coggin, D. K.; Vincent, J. B.; McCusker, J. K.; Streib,
W. E.; Huffman, J. C.; Hendrickson, D. N.; Christou, G. *J. Chem.
Soc., Dalton Trans.* **1998**, 719.
(25) Castro, S. L.; Sun, Z.; Bollinger, J. D.; Hendrickson, D. N.; Christou,
G. *J. Chem. Soc., Chem. Commun.* **1995**, 2517.
(26) Libby, E.; McCusker, J. K.; Schmitt, E. A.; Folting, K.; Hendrickson,
D. N.; Christou, G. *Inorg. Chem.* **1991**, *30*, 3486.

Table 2. Selected Interatomic Distances (Å) and Bond Angles (deg) for Complex **1**

Fe1−O1	1.9170(13)	Fe3−O1	1.9330(12)
Fe1−O2	2.0238(14)	Fe3−O5	2.0007(15)
Fe1−O4	2.0149(14)	Fe3−O7	1.9986(14)
Fe1−O6	2.0328(13)	Fe3−O9	1.9778(15)
Fe1−O12	1.9776(14)	Fe3−O11	2.0187(14)
Fe1−N1	2.2034(16)	Fe3−O16	2.0981(13)
Fe2−O1	1.8972(14)	Na−O12	2.5460(17)
Fe2−O3	2.0223(14)	Na−O13	2.4895(18)
Fe2−O8	2.0095(14)	Na−O14	2.5277(15)
Fe2−O10	2.0026(14)	Na−O15	2.5389(18)
Fe2−O14	1.9948(14)	Na−O17	2.4488(16)
Fe2−N2	2.1852(17)	Na−O18	2.3550(17)
		Na−O15′	2.3436(16)
Fe1···Fe2	3.3703(5)	Fe1···Na	4.3714(8)
Fe1···Fe3	3.2846(4)	Fe2···Na	4.3607(8)
Fe2···Fe3	3.2829(5)	Na···Na′	3.6990(17)
O2−Fe1−O12	90.93(6)	O3−Fe2−O14	89.80(6)
O2−Fe1−N1	86.33(6)	O3−Fe2−N2	89.64(6)
O4−Fe1−O6	91.71(6)	O8−Fe2−O10	93.58(6)
O4−Fe1−O12	162.13(6)	O8−Fe2−O14	87.50(6)
O4−Fe1−N1	84.58(6)	O8−Fe2−N2	82.84(6)
O6−Fe1−O12	86.91(6)	O10−Fe2−O14	160.28(6)
O6−Fe1−N1	81.55(6)	O10−Fe2−N2	83.68(6)
O1−Fe1−O2	95.73(6)	O1−Fe2−O3	95.18(6)
O1−Fe1−O4	97.02(5)	O1−Fe2−O8	92.33(6)
O1−Fe1−O6	96.40(5)	O1−Fe2−O10	97.74(6)
O1−Fe1−O12	100.84(6)	O1−Fe2−O14	101.89(6)
O1−Fe1−N1	177.45(5)	O1−Fe2−N2	175.05(5)
O2−Fe1−O4	86.69(6)	O3−Fe2−O8	172.41(6)
O2−Fe1−O6	167.87(6)	O3−Fe2−O10	86.59(6)
O12−Fe1−N1	77.59(6)	O14−Fe2−N2	76.91(6)
O1−Fe3−O5	95.58(6)	O11−Fe3−O16	82.21(6)
O1−Fe3−O7	96.80(5)	O5−Fe3−O11	86.98(6)
O1−Fe3−O9	93.56(6)	O5−Fe3−O16	84.98(6)
O1−Fe3−O11	98.44(5)	O7−Fe3−O9	89.06(6)
O1−Fe3−O16	179.16(5)	O7−Fe3−O11	164.72(5)
O5−Fe3−O7	90.50(6)	O7−Fe3−O16	82.56(5)
O5−Fe3−O9	170.84(5)	O9−Fe3−O11	91.05(6)
		O9−Fe3−O16	85.89(6)
O12−Na−O13	52.25(5)	O13−Na−O15′	101.27(6)
O12−Na−O14	71.76(5)	O14−Na−O15	52.10(5)
O12−Na−O15	123.51(5)	O14−Na−O17	95.65(6)
O12−Na−O17	93.08(6)	O14−Na−O18	94.47(6)
O12−Na−O18	109.03(6)	O14−Na−O15′	133.62(6)
O12−Na−O15′	153.22(6)	O15−Na−O17	87.10(6)
O13−Na−O14	123.67(5)	O15−Na−O18	83.47(6)
O13−Na−O15	168.61(6)	O15−Na−O15′	81.57(6)
O13−Na−O17	82.77(6)	O17−Na−O18	157.64(7)
O13−Na−O18	107.83(6)	O17−Na−O15′	77.77(6)
O18−Na−O15′	80.81(6)		
Fe1−O1−Fe2	124.16(6)	Fe1−O12−Na	149.95(7)
Fe1−O1−Fe3	117.11(7)	Fe2−O14−Na	149.02(8)
Fe2−O1−Fe3	117.98(6)	Na−O15−Na′	98.43(6)

solution, from which orange prisms of **1**·2EtOH precipitated. The reaction leading to the isolation of this complex can be summarized by eq 2.

$$6Fe(ClO_4)_3 \cdot 6H_2O + 10NaO_2CPh + 4Napic +$$
$$4EtOH \xrightarrow[\text{reflux}]{\text{EtOH}} [Fe_6O_2(O_2CPh)_{10}(pic)_4Na_2(EtOH)_4(H_2O)_2]$$
$$(ClO_4)_2 + 4HClO_4 + 12NaClO_4 + 32H_2O \quad (2)$$

Description of the Structure. The complex crystallizes in the $P\bar{1}$ space group. Selected interatomic distances and

angles are shown in Table 2. It consists of one complex cation, two perchlorate anions, and two ethanol solvate molecules. The latter two will not be further discussed. The complex cation is centrosymmetric and contains two symmetry-related {Fe$_3$O(O$_2$CPh)$_5$(pic)$_2$(H$_2$O)} subunits, related to each other by an inversion center ($-x$, $-y$, $1 - z$), situated between the two sodium atoms. Inside each subunit, the three iron atoms are held together by one μ_3-oxide and five syn− syn μ-benzoate bridges. This bridging mode is reminiscent of that in [Fe$_3$O(O$_2$CMe)$_7$(OH$_2$)](Et$_4$N).[27]

In the following description, only one subunit (x, y, z) will be explicitly examined. The two subunits are bridged by the two sodium cations, through two $\mu_3:\eta^1:\eta^2:\eta^2$ (or 3.221 using Harris' notation[28]) and two $\mu:\eta^1:\eta^2:\eta^2$ (or 2.211 using Harris' notation) bridging chelating picolinate anions. The first picolinate ligand is coordinated to Fe2, Na, and Na′, whereas the second is coordinated to Fe1 and Na.

The iron cations are in distorted-octahedral coordination environments with NO$_5$ donor sets for Fe1 and Fe2 and a O$_6$ donor set for Fe3. The Fe−L bonds are in the range 1.917(12)−2.203(13) Å for Fe1, 1.897(7)−2.185(7) Å for Fe2, and 1.933(9)−2.098(9) Å for Fe3. The shortest bonds are the Fe−O1$_{oxo}$ ones, whereas the longest ones are those in the position trans to O1 (trans effect). The Fe$_3$O core is planar, with an Fe−O−Fe angle sum of 359.26°.

The coordination around the sodium atoms is distorted-pentagonal bipyramidal, with O12, O13, O14, O15, and O15′ equatorial and O17 and O18 axial donor atoms. The Na−O bond lengths span the range 2.344(19)−2.546(14) Å.

The complex cation presents an almost planar central core, defined by atoms Fe1, Fe2, Na, Fe1′, Fe2′, and Na′, with the defining atoms very close to the mean plane and with the symmetry-related atoms on opposite sides of this mean plane. Thus, Fe1 is situated 0.065 Å below the plane, whereas Fe2 and Na are 0.034 and 0.145 Å above the plane, respectively. Atoms Fe3 and Fe3′ are situated 2.025 Å above and below the mean plane, respectively. This plane forms angles of 133.57° with the planes defined by atoms Fe1/Fe2/Fe3 and Fe1′/Fe2′/Fe3′ (Figure 1).

Magnetic Properties. For complex **1**, the value of the product $\chi_M T$ (9.12 cm^3 mol^{-1} K^{-1} at 300 K) is significantly lower than the theoretically expected one for three noninteracting $S = \frac{5}{2}$ spins (26.28 cm^3 mol^{-1} K^{-1}), indicating antiferromagnetic interactions, as is also suggested by the drop of $\chi_M T$ upon cooling (Figure 2). Below 20 K, the $\chi_M T$ product shows deviations from the theoretical curve, which is attributed to the combined effects of a small fraction of an $S = \frac{5}{2}$ paramagnetic impurity and non-Heisenberg interactions, as is established by EPR experiments (see EPR Spectrocopy section).

Consideration of the molecular symmetry of **1** would suggest that four exchange parameters have to be taken into account in order to describe the magnetic behavior of **1**: $J_A = J_{13} = J_{1'3'}$, $J_B = J_{23} = J_{2'3'}$, $J_C = J_{12} = J_{1'2'}$, and $J_D = J_{12'}$

(27) Reynolds, R. A., III; Dunham, W. R.; Coucouvanis, D. *Inorg. Chem.* **1998**, *37*, 1232.
(28) Coxall, R. A.; Harris, S. G.; Henderson, D. K.; Parsons, S.; Tasker, P. A.; Winpenny, R. E. P. *J. Chem. Soc., Dalton Trans.* **2000**, 2349.
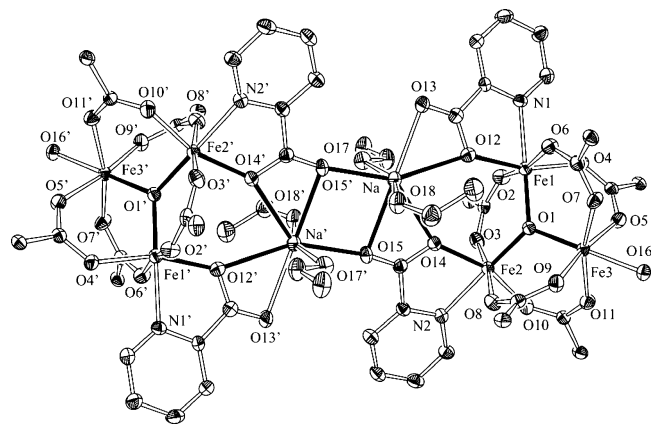
Figure 1. ORTEP diagram of the complex cation of **1** at the 30% probability level. Hydrogen atoms, as well as the carbon atoms of the benzoate phenyl rings (except for those at the 1 positions), have been omitted for clarity.
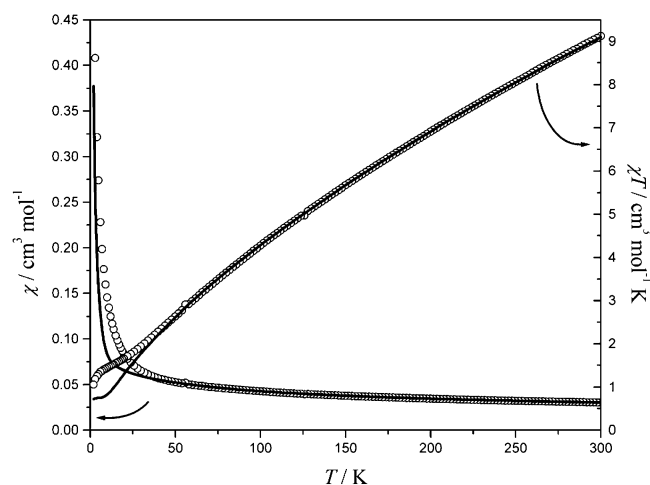

Figure 2. χ_M vs T and $\chi_M T$ vs T experimental data for complex **1** and theoretical curves based on the Hamiltonian of eq 3.
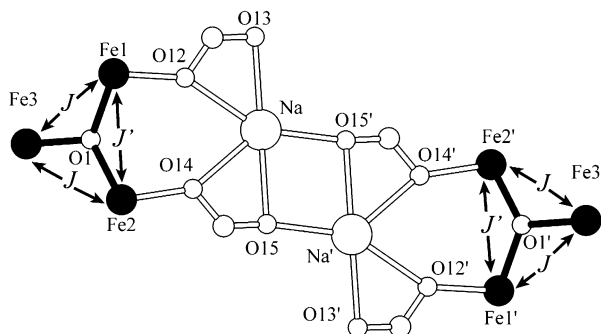
Figure 3. Spin-coupling scheme for complex **1**.

$= J_{1'2}$. A closer examination of the molecular geometry, however, allows for simplifications; the large separation of the Fe_3O subunits allows us to safely assume that they do not interact (see Figure 3). Indeed, Fe1 and Fe2' are separated by six bonds and five diamagnetic atoms, allowing one to consider that $J_D = 0$. Consequently, we consider the complex to comprise two noninteracting Fe_3O cores. EPR spectroscopy presented later also supports the presence of noninteracting paramagnetic cores.

In addition, an examination of the Fe···Fe distances and the Fe−O1−Fe angles indicates that Fe−Fe interactions
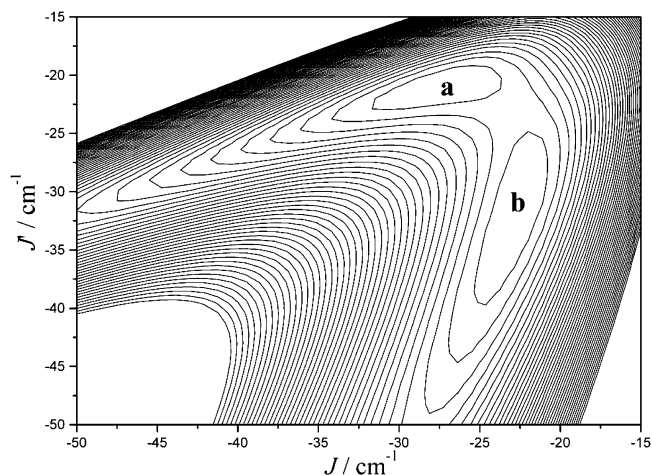
Figure 4. Surface error plot of J vs J' (with $g = 2.00$) revealing the minima **a** ($R = 9.3 \times 10^{-6}$) and **b** ($R = 5.9 \times 10^{-5}$) found by the fitting process.

can be subdivided into two groups: the first one includes Fe1−Fe3 and Fe2−Fe3 [Fe1···Fe3, 3.2846(4) Å, Fe1−O1−Fe3, 117.11(7)°; Fe2···Fe3, 3.2829(5) Å, Fe2−O1−Fe3, 117.98(6)°], while the second one involves Fe1−Fe2 [Fe1···Fe2, 3.3703(5) Å, Fe1−O1−Fe2, 124.16(6)°]. We can thus consider that $J_{13} = J_{23} = J_{1'3'} = J_{2'3'} = J$ and $J_{12} = J_{1'2'} = J'$. On the basis of that above, the Hamiltonian of the system can be written as

$$\hat{H} = -2J(\hat{S}_1\hat{S}_3 + \hat{S}_2\hat{S}_3 + \hat{S}_1\hat{S}_{3'} + \hat{S}_2\hat{S}_{3'}) - 2J'(\hat{S}_1\hat{S}_2 + \hat{S}_1\hat{S}_{2'}) \quad (3)$$

Fitting of the data was carried out over the 50−300 K temperature range to reliably determine the sizes of the J couplings. Below 50 K, the combined effects of a small fraction of ferric paramagnetic impurity ($S = {}^5/_2$; also confirmed by EPR spectroscopy; see below) and non-Heisenberg interactions made it impossible to obtain reliable fits, and thus the paramagnetic impurity is not considered. Fits of the experimental data with the expression of the susceptibility based on the above spin Hamiltonian yielded two satisfactory sets of parameters: (**a**) $J = -27.4$ cm^{-1}, $J' = -20.9$ cm^{-1}, and $g = 2.0$ (fixed) and (**b**) $J = -22.7$ cm^{-1}, $J' = -31.6$ cm^{-1}, and $g = 2.0$ (fixed). Obtaining two minima upon fitting of the magnetic susceptibility data of trinuclear clusters is not unusual.[29] In our case, this is illustrated in Figure 4, where we show in a two-dimensional plot the dependence of the error factor R on the values J and J'. On the basis of the best-fit parameters, susceptibility curves were calculated for the full temperature range (2−300 K) in order to compare the calculated with the experimental curves. Below 50 K, the calculated curves fall below the experimental data because the paramagnetic impurity was not considered. However, at the high-temperature region, the agreement was excellent. The fit obtained from solution **a** was of superior quality and is shown in Figure 2. Energy level plots for both fits reveal an $S = {}^1/_2$ ground state.

(29) (a) Long, G. J.; Robinson, W. T.; Tappmeyer, W. P.; Bridges, D. L. J. *J. Chem. Soc., Dalton Trans.* **1973**, 573. (b) Jones, D. H.; Sams, J. R.; Thompson, R. C. *J. Chem. Phys.* **1984**, *81*, 440.
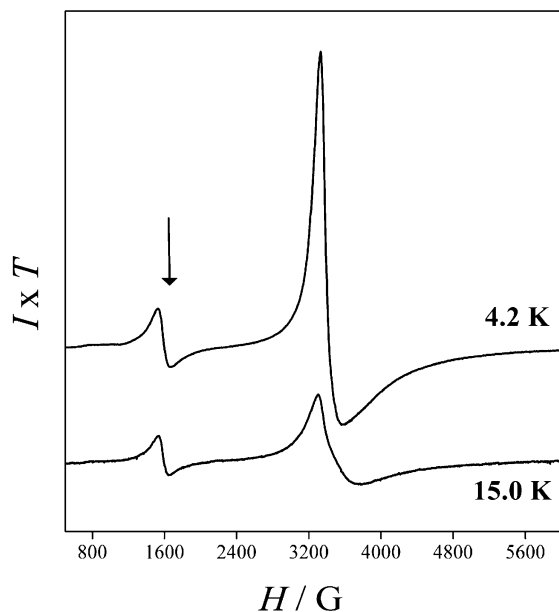
Figure 5. X-band EPR spectra of **1** in polycrystalline form at 4.2 and 15 K. The arrow indicates the signal at $g \sim 4.3$ attributed to $S = {}^5/_2$ impurities. EPR conditions: microwave power, 2 mW; model amplitude, 10 G_{pp}; microwave frequency, 9.41 GHz.

Figure 6. X-band EPR spectra of **1** in an acetone glass at various temperatures. EPR conditions are as in Figure 6. Arrows in the 15 and 21 K spectra denote signals arising from the EPR cavity.

Examination of the intermetallic Fe···Fe distances reveals that for the pairs Fe1/Fe3 and Fe2/Fe3 the distance is shorter compared to the Fe1/Fe2 pair, and it might be expected to lead to stronger interactions (solution **a**). However, a definite choice of solution (**a** or **b**) would be questionable for reasons discussed in the analysis of the EPR and Mössbauer data presented below. Nevertheless, the order of magnitude for the values of the exchange interactions in both cases falls within the range expected for exchange-coupled systems involving high-spin ferric ions bridged through oxo and carboxylato moieties.[3a,c,29a,30]

EPR Spectroscopy. To further describe the magnetic properties of **1**, we carried out an EPR study at the X band. We performed measurements both in the solid state (microcrystalline powder; Figure 5) and in an acetone glass (Figure 6). The powder spectra consist of two signals at $g = 4.3$ and at $g \sim 2.0$. The former follows roughly the Curie temperature law and is readily assigned to an iron(III), $S = {}^5/_2$, monomeric impurity. Accurate quantitations for such species cannot be obtained. We estimate, however, that these species cannot account for more than 6% of the spins. The strong asymmetric signal at $g \sim 2.0$ is compatible with a system possessing an $S = {}^1/_2$ ground state and is attributed to complex **1**. The spectral characteristics are in agreement with the magnetic susceptibility data, which were analyzed, assuming two noninteracting triads. At higher temperatures, the signal decreases and a significant broadening is observed (Figure 6).

To avoid solid-state effects, we studied also **1** in an acetone glass (Figure 6). As in the powder spectrum, a strong asymmetric signal at $g \sim 2.0$ is observed at 4.2 K, indicating that the trimeric form is retained in solution. A closer
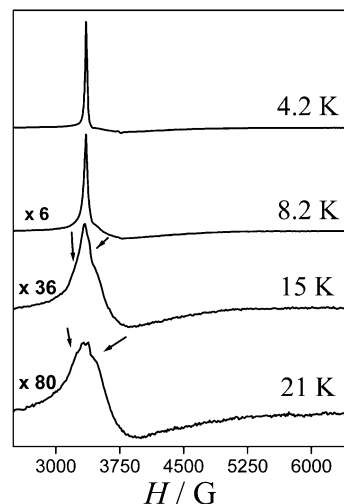
(30) Duncan, J. F.; Kanekar, C. R.; Mok, K. F. *J. Chem. Soc., A* **1969**, 480.

examination of the spectra reveals that the signal consists of a rather sharp absorption peak at a g value very close to 2.00 and a very broad high-field tail. We studied the concentration effects on the EPR spectra of the complex, and the spectra shown in Figure 6 correspond to the limit of no dependence on the concentration.

It could be expected that weak interactions (mainly of dipolar origin) between the two {Fe₃O} units of the molecule are responsible for the EPR behavior shown in Figure 6. We have carried out theoretical simulations involving two $S = {}^1/_2$ species with isotropic g tensors (2.0) interacting through weak anisotropic exchange interactions. In the limiting case of zero magnetic interactions, a symmetric line at $g \sim 2.0$ is induced. Introduction of anisotropic interactions induces splitting of this line, yielding features at $g > 2.0$ and $g < 2.0$.[31] Clearly, this is not the case in the spectra of Figure 6. The sharp peak at $g = 2.0$ and the broad tail at higher field suggest that the $S = {}^1/_2$ ground state of the system is characterized by an anisotropy with three different g components (g_1, g_2, and g_3). This is a common feature to many trinuclear complexes comprising Kramers ions. The line shape of the spectra suggests one well-defined g_1 value corresponding to the sharp absorption peak, whereas the other g values exhibit significant g-strain effects. For reasons discussed below, we assume axial anisotropy, namely, $g_2 = g_3 = g_\perp$. We further assume a distribution of such species by calculating a large number of axial spectra with $g_1 = 2.00$ and $g_\perp < 2.0$. Then, by a least-squares fit routine, we determine the contribution of each spectrum to the experimental one. Indicative results for the spectrum at 8 K are shown in Figure 7, with the contribution of each axial species shown in the inset. In Figure S1 in the Supporting Information, we show the distributions obtained from spectra recorded at different temperatures. For each case, a relatively broad maximum is observed at $g \sim 1.70$. We conclude, therefore, that the ground state of the system comprises an axial $S = {}^1/_2$ system with $g_\| = 2.00$ and $g_\perp \sim 1.70$.

In the case of iron(III) ($S = {}^5/_2$) trimers, because the intrinsic g tensor is isotropic (close to 2.00), the anisotropy
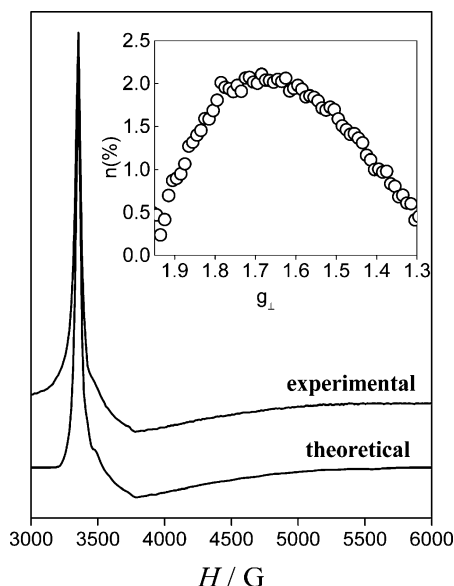
Figure 7. Simulation of the 8 K spectrum of **1** in an acetone glass (Figure 6). Inset: distribution of the axial species resulting from the simulation procedure described in the text.
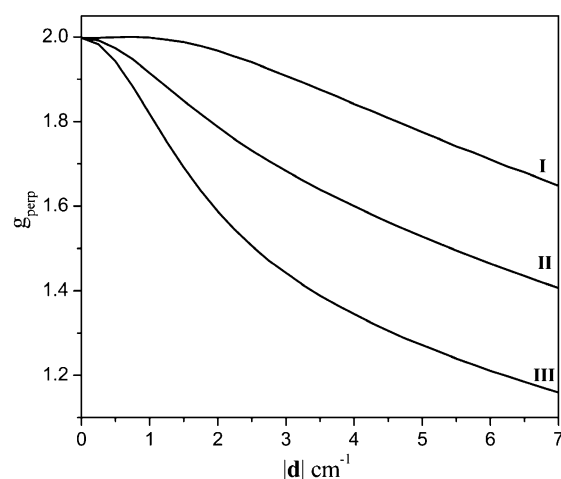
in the ground state of the exchange-coupled trimer originates from non-Heisenberg exchange interactions and single-ion ZFS terms. The non-Heisenberg interactions include dipolar and pseudo-dipolar exchange interactions and AE, as mentioned in eq 4,

$$\hat{H}_{NH} = \hat{H}_{ZFS} + \hat{H}_{dip} + \hat{H}_{anti} = \sum \hat{S}_i \mathbf{D}_i \hat{S}_i +$$
$$\sum \hat{S}_i \mathbf{D}_{ij} \hat{S}_j + \mathbf{d} \cdot (\sum \hat{S}_i \times \hat{S}_j) \qquad i, j = 1-3 \quad (4)$$

where **d** is a pseudovector perpendicular to the plane of the triangle and the other symbols have their usual meaning.

The effect of the single-ion ZFS on the EPR spectra of iron(III) trinuclear species ($S = {}^5/_2$) has been studied by Guigliarelli et al.[32] In the $S = {}^1/_2$ ground state, the ZFS term mixes higher states with $S \neq {}^1/_2$ to the $S = {}^1/_2$ one. A perturbation treatment of this term on the pure states resulting from the isotropic Heisenberg interactions shows that the g-tensor anisotropy depends on the ratio $|D|/J$. The anisotropic exchange interactions (dipolar and pseudo-dipolar) also depend on the ratio $|D_{ij}|/J$. For a non-heme ferric ion in an environment comprising N and O, usually $|D|$ is smaller than $\sim 3-4$ cm^{-1}. From the geometry of cluster **1**, we estimate that the dipolar interaction is on the order of ~ 1 cm^{-1}. Because the J_{ij} values have been determined from the magnetic susceptibility measurements, we may estimate the contribution of each term to the anisotropy of the EPR spectra. It can then be seen that the contributions of the ZFS and dipolar terms are too small to account for the observed anisotropy.

On the other hand, AE is more critical because it mixes the two $S = {}^1/_2$ states. The effect of this term is to induce

---

(31) Representative theoretical spectra can be found in: Boudalis, A. K.; Sanakis, Y.; Raptopoulou, C. P.; Terzis, A.; Tuchagues, J.-P.; Perlepes, S. P. *Polyhedron* **2005**, *24*, 1540.

(32) 2 Guigliarelli, B.; More, C.; Bertrand, P.; Gayda, J.-P. *J. Chem. Phys.* **1986**, *85*, 2774. (b) Guigliarelli, B.; Gayda, J.-P.; Bertrand, P.; More, C. *Biochim. Biophys. Acta* **1986**, *871*, 149.

Figure 8. Dependence of g on the antisymmetric parameter |**d**| for three J_{ij} triads. The theoretical curves were obtained for $(J_{12}, J_{13}, J_{23}) = (-21, -27.5, -27.5)$ cm^{-1} (**I**), $(-21.5, -21.5, -27)$ cm^{-1} (**II**), and $(-22, -22, -26.5)$ cm^{-1} (**III**).

axial anisotropy ($g_x = g_y = g_\perp \neq g_z = g_{\|}$). The orientation of the g tensor is such that the parallel component, $g_{\|}$, coincides with the **d** pseudovector, which is perpendicular to the triangular plane, whereas the perpendicular component, $g_\perp$, lies on the triangular plane. It is found that $g_{\|}$ is, to first order, independent of |**d**|, whereas $g_\perp$ depends on the ratio $|\mathbf{d}|/\delta$, where δ reflects the energy difference of the two lowest $S = {}^1/_2$ states and it is given by the relationship $\delta = 6|J - J'|$. In this context, the relatively sharp peak at $g \sim 2.0$ observed in the spectra is attributed to the $g_{\|}$ component of the axial tensor and the broad maximum at ~ 1.70 to the $g_\perp$ component. In Figure 8, we plot the dependence of $g_\perp$ on |**d**| for three cases of J_{ij} triads close to solution **a**, namely, **I** (-21, -27.5, and -27.5 cm^{-1}), **II** (-21.5, -27, and -27 cm^{-1}), and **III** (-22, -26.5, and -26.5 cm^{-1}).[33] From this plot, the g-tensor anisotropy can be accounted for by a |**d**| value in the 2.0$-$4.0-cm^{-1} range. These values compare with those determined by Mössbauer spectroscopy for the diferric pair of the hydroxylase component of methane monooxygenase and a synthetic analogue[35] as well as other carboxylate-bridged triferric complexes.[6a]

To reproduce the line shapes at the high-field region of the spectra, we used an apparent distribution of the $g_\perp$ values. The line shape is temperature-dependent (Figures 6 and S1 in the Supporting Information) and may be partly attributed to spin relaxation or other dynamic effects. Pulsed EPR or

---

(33) Analytical expressions for the dependence of $g_\perp$ on |**d**| for {Fe$^{III}_3$} species have been derived by a perturbation treatment involving only the two lowest $S = {}^1/_2$ states.[6a,12] This approach is sufficient when the energy difference between the two lowest $S = {}^1/_2$ states and the $S > {}^1/_2$ states is large. For instance, this is the case for the [3Fe$-$4S]$^+$ cuboidal clusters in proteins.[34] In the present case, the inequivalence of J_{ij} is such that the first $S = {}^3/_2$ manifold is very close to the first excited $S = {}^1/_2$ state, implying that the analytical expressions cannot be applied. The results plotted in Figure 9 have been obtained using a home-written program, which numerically diagonalizes eq 4 by taking into consideration the manifolds with S up to ${}^5/_2$.

(34) (a) Day, E. P.; Peterson, J.; Bonvoisin, J.-J.; Moura, I.; Moura, J. J. G. *J. Biol. Chem.* **1988**, *263*, 3684. (b) Macedo, A. L.; Moura, I.; Moura, J. J. G.; LeGall, J.; Huyhn, B. H. *Inorg. Chem.* **1993**, *32*, 1101.

(35) Kauffmann, K. E.; Popescu, C. V.; Dong, Y. H.; Lipscomb, J. D.; Que, L.; Munck, E. *J. Am. Chem. Soc.* **1998**, *120*, 8739.
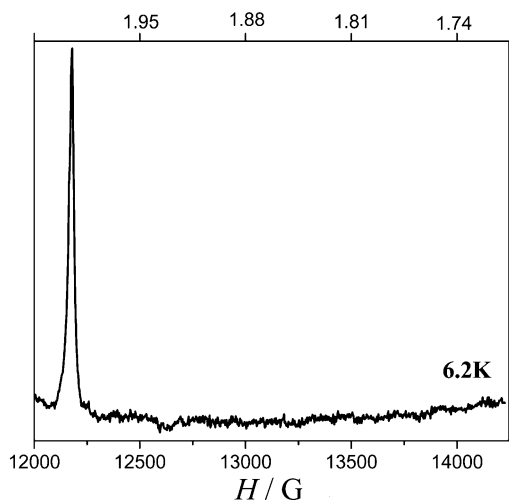
Figure 9. Q-band EPR spectra of **1** in an acetone glass at 6.2 K. EPR conditions: microwave power, 0.2 mW; model amplitude, 5 G_{pp}; microwave frequency, 34.2 GHz.

Figure 10. Zero-field Mössbauer spectra of **1** at selected temperatures. Solid lines represent fitted spectra assuming one asymmetric quadrupole-split doublet.

vibrational techniques are required to study such phenomena. Another possibility is that this $g_\perp$ distribution reflects distributions in the parameters $|\mathbf{d}|$ and J_{ij}. The presence of such distributions is supported by the Mössbauer results to be presented below. From Figure 8, we observe that the $g_\perp$ component is extremely sensitive on the pseudovector $|\mathbf{d}|$ and on the exchange coupling constants, J_{ij}'s. For instance, for $|\mathbf{d}| \sim 3.0$ cm^{-1}, a distribution of J_{ij}'s on the order of only 2.5% would induce a severe distribution of the $g_\perp$ component. Thus, the pertinent EPR spectrum is expected to give rise to a sharp, $g_{||}$, absorption peak and a broad high-field tail corresponding to the distributed $g_\perp$ values, as is observed in the present case.

Experiments performed at the Q band support the model of an $S = \frac{1}{2}$ system exhibiting axial anisotropy with a well-defined $g_{||}$ component and a severely distributed $g_\perp$ component. In Figure 9, we show a Q-band EPR spectrum from an acetone glass of **1** at 6.2 K. In the $g \sim 2.0$ region, a strong absorption peak is observed with a very broad high-field tail. From the analysis of the X-band spectra, the $g \sim 2.0$ feature corresponds to the $g_{||}$ component of the $S = \frac{1}{2}$ species. The $g_\perp$ component is widely distributed with a broad maximum at $g \sim 1.70$. Unfortunately, our instrumental limitations do not allow us to record spectra at higher magnetic fields so as to monitor features corresponding to $g < 1.65$ revealed at the X-band spectra.

Mössbauer Spectroscopy. (a) Zero-Field Mössbauer Spectra. The Mössbauer spectra of complex **1** at various temperatures in the absence of an external magnetic field are shown in Figure 10. In general, the spectra consist of a relatively broad doublet in the whole temperature range. We have simulated these spectra with a quadrupole-split doublet, allowing for different line widths for the lower and higher energy peaks. The obtained parameters, quoted in Table S1 in the Supporting Information, are typical for high-spin iron-(III) in an octahedral environment comprising N/O ligands. The molecular structure of the complex reveals that it contains two iron sites with FeO$_5$N (Fe1 and Fe2) and FeO$_6$ (Fe3) chromophores in a 2:1 ratio, respectively. Therefore,
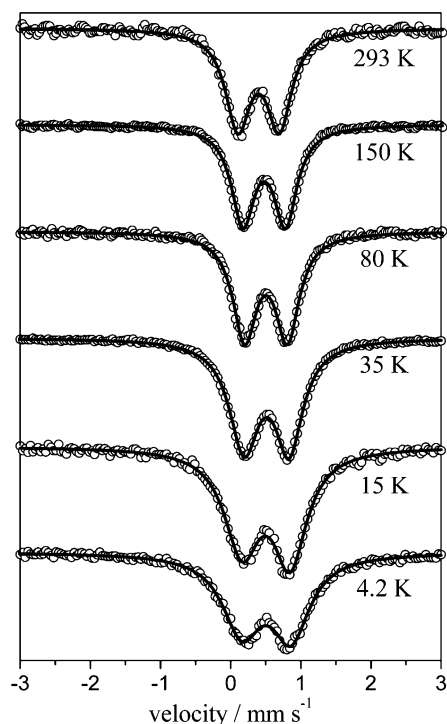
we would expect the appearance of a composite quadrupole-split doublet. However, this is not the case in the spectra of Figure 10. For $T > 75$ K, we obtain a symmetric quadrupole-split doublet with a relatively broad line width ($\Gamma_{1/2} \sim 0.20$ mm s^{-1}), which is significantly larger than the limit of our experimental setup (ca. 0.13 mm s^{-1}). The quadrupole splitting does not depend significantly on the temperature for $T > 75$ K, whereas the decrease of the isomer shift upon heating is attributed to a second-order Doppler effect.[36]

As the temperature is decreased below 75 K, the lines broaden gradually with an apparent increase of the quadruple splitting. For $T < 20$ K, an asymmetry is observed, with the left line being broader than the right one. At 4.2 K, a broad doublet is observed ($\Gamma_{1/2} \sim 0.34$ mm s^{-1}). The temperature dependence of the line width and the asymmetry of the doublet at low temperatures indicate the onset of relaxation effects, as has been observed in other trinuclear ferric carboxylate complexes.[37]

(b) Mössbauer Spectra at 4.2 K in the Presence of External Magnetic Fields. The 4.2 K spectra in the presence of external magnetic fields applied perpendicularly to the γ-rays are shown in Figure 11. The spectra consist of relatively broad absorptions confined in the −5 to +5 mm s^{-1} region. Clearly, the spectra cannot be reproduced by assuming isolated high-spin ferric species, in agreement with the aforementioned magnetic and EPR studies, indicating a {Fe^{III}}$_3$ coupled system with an $S = \frac{1}{2}$ ground state. From the EPR measurements presented above, the presence of a

(36) Greenwood, N. N.; Gibbs, T. C. *Mössbauer Spectroscopy*; Chapman and Hall: New York, 1971; pp 9−11 and 50−53.
(37) Filoti, G.; Meriacre, V. M.; Mateescu, E.; Kuncser, V.; Turta, K. I. *Hyperfine Interact.* **1998**, *116*, 127.
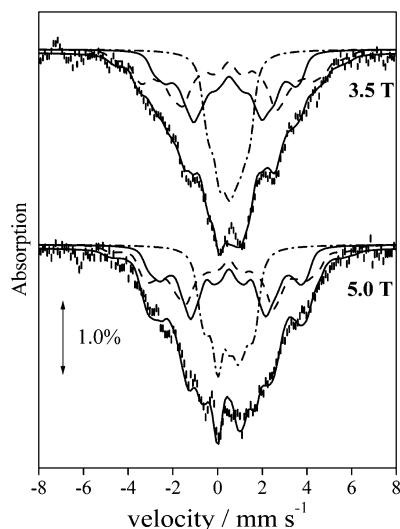
Figure 11. 4.2 K Mössbauer spectra of **1** in the presence of external magnetic fields applied perpendicularly to the γ irradiation. Solid lines represent theoretical curves obtained with the parameters quoted in Table 3. The contributions of each site are also shown.

high-spin ferric paramagnetic impurity was indicated, accounting for less than 2% of the total iron (equivalent to a 6% fraction of total spins because we consider a trinuclear species). This amount is too small to yield a significant contribution in the magnetically perturbed Mössbauer spectra and should not affect the analysis presented below.

The Mössbauer properties of coupled trinuclear iron(III) complexes have been discussed earlier.[38] For each iron site, the total magnetic field is given by the relationship

$$\mathbf{H}_i = \mathbf{H}_{ext} - c_i\langle \mathbf{S}\rangle \frac{\mathbf{a}_i}{g_N\beta_N} \qquad i = 1-3 \qquad (5)$$

where $\langle \mathbf{S}\rangle$ is the expectation value of total spin **S** and $\mathbf{a}_i$ is the intrinsic hyperfine tensor for each iron. For iron(III) ($S = {}^5/_2$), $\mathbf{a}_i$ is isotropic, and in an octahedral environment comprising N/O ligands, this value is ca. -30 MHz. In the presence of external magnetic fields, the expectation values for the ground state are $\langle S_x\rangle = \langle S_y\rangle = \langle S_z\rangle = -{}^1/_2$. c_i is a projection coefficient that depends critically on the relationship between the J_{ij} values.[39] In the context of the isotropic HDvV Hamiltonian alone (eq 1), the internal magnetic fields $c_i\langle \mathbf{S}\rangle\mathbf{a}_i$ are isotropic. We have analyzed the spectra by assuming three subsites with a $S = {}^1/_2$ Hamiltonian (eq 6) and effective hyperfine tensors $\mathbf{A}_i = c_i\mathbf{a}_i$.

$$H = \beta\mathbf{B}\cdot\tilde{\mathbf{g}}\cdot\mathbf{S} + \mathbf{S}\cdot\tilde{\mathbf{A}}_i\cdot\mathbf{I} - g_n\beta_n\mathbf{B}\cdot\mathbf{I} + \frac{eQV_{zz}}{12}[3I_z^2 - I(I+1) + n(I_x^2 - I_y^2)] \quad (6)$$

In eq 6, all symbols have their conventional meaning. The g tensor was taken as isotropic ($g = 2.00$); variation of the g tensor has a small effect on the simulations.

At 4.2 K, the lowest $S = {}^1/_2$ ground state is almost 100% populated, and hence the Mössbauer spectra can be analyzed by considering this doublet only. In the following, we discuss the simulations obtained in the slow relaxation regime.[40] In Figure 11, continuous lines superimposed on the experimen-

Table 3. Hyperfine Parameters for the Three Ferric Sites Used To Simulate the Magnetically Perturbed Mössbauer Spectra at 4.2 K (Figure 11)

| site	δ^a (mm s^{-1})	$\Delta E_Q{}^a$ (mm s^{-1})	$A_x{}^b$ (MHz)	$A_y{}^b$ (MHz)	$A_z{}^b$ (MHz)	A_{iso} (MHz)
1	0.51	0.70	-41.2	-78.2	-80.5	$-67(3)$
2	0.51	0.70	$+20.2$	$+45.9$	$+43.5$	$+36(3)$
3	0.51	0.70	$+0.76$	$+5.06$	$+3.29$	$+3(3)$

^{a} Taken from the zero-field spectra at 4.2 K (Table 3). ^{b} See the text for derivation of these parameters.

tal spectra (hash marks) represent theoretical simulations based on eq 6. For the simulations, we used the isomer shifts and quadrupole splittings derived from the zero-field spectra at 4.2 K. We also assumed that the ferric sites have common EFG tensors collinear with the hyperfine tensors. The best simulations were obtained for $\eta = 0.9$ with the hyperfine parameters quoted in Table 3. The quoted hyperfine parameters are quite tentative and certainly not unique. It is clear, however, that the features of the experimental spectra cannot be reproduced by assuming isotropic $\mathbf{A}_i$ tensors for the three ferric sites and reasonable line widths. In Table 3, we quote also the obtained isotropic values $[A_{iso,i} = (A_{x,i} + A_{y,i} + A_{z,i})/3]$ for each iron site. Although the components $A_{x,i}$, $A_{y,i}$, and $A_{z,i}$ cannot be uniquely determined from the simulations, we find that the isotropic values $A_{iso,i}$ can be safely estimated with the errors quoted in Table 3. If we assume that the intrinsic hyperfine tensors $\mathbf{a}_i$ are equal for the three ferric sites, the relationship of $A_{iso,i}$ and a_i is such that $\sum A_{iso,i} = a_i$. From the values of Table 3, we find that in our case $a_{in} = -28$ MHz. With the experimental uncertainties, this value is close to the value expected for ferric ions in an octahedral environment comprising O/N atoms.

The fact that the spectra cannot be reproduced with isotropic $\mathbf{A}_i$ values is not expected in a coupled system involving high-spin ferric ions and in the context of the isotropic H_{HDvV} Hamiltonian.

From the EPR spectroscopic results presented above, it was concluded that AE has to be included in order to interpret the EPR spectra. The role of AE in the Mössbauer spectra from trinuclear clusters was examined theoretically[41] and

(38) (a) Takano, M. *J. Phys. Soc. Jpn.* **1972**, *33*, 1312. (b) Rumbold, B. D.; Wilson, G. V. H. *J. Phys. Chem. Solids* **1973**, *34*, 1887. (c) Kent, T. A.; Hyhn, B. H.; Münck, E. *Proc. Natl. Acad. Sci. USA* **1980**, *77*, 6574. (d) Tsukerblat, B. S.; Filoti, G.; Bartolome, J.; Dickson, D. P. E.; Rillo, C.; Prisecaru, I.; Jovmir, T.; Kuncser, V.; Turta, C. *J. Magn. Magn. Mater.* **1999**, *196–197*, 561.

(39) (a) Bencini, A.; Gatteschi, D. *EPR of Exchanged Couple Systems*; Springer-Verlag: Berlin, 1990. (b) Kent, T. A.; Huynh, B. H.; Munck, E. *Proc. Natl. Acad. Sci. USA* **1980**, *77*, 6574.

(40) Upon application of an external magnetic field, the $S = {}^1/_2$ state splits into two states characterized by $S_z = \pm^1/_2$. In the slow-relaxation limit, the spectrum of each iron consists of two magnetic subspectra from the states that correspond to $S_z = -{}^1/_2$ and $+{}^1/_2$. Each subspectrum contributes according to the thermal occupation of each state. The occupation of the state with $S_z = -{}^1/_2$ is ~75% and ~83% at 3.5 and 5.0 T, respectively. In the fast-relaxation regime, the spectrum for each iron depends on the thermal average $\langle \mathbf{S}\rangle_{th}$ of **S**. At 3.5 T, $\langle \mathbf{S}\rangle_{th} = -0.253$, and at 5.0 T, $\langle \mathbf{S}\rangle_{th} = -0.332$. We cannot be definite about the relaxation conditions pertinent to the spectra of Figure 11. However, we have analyzed the spectra assuming both regimes, and the information obtained from this analysis converges to the same conclusions.

(41) Fainzilberg, V. E.; Belinski, M. I.; Tsukerblat, B. S. *Mol. Phys.* **1981**, *44*, 1195.
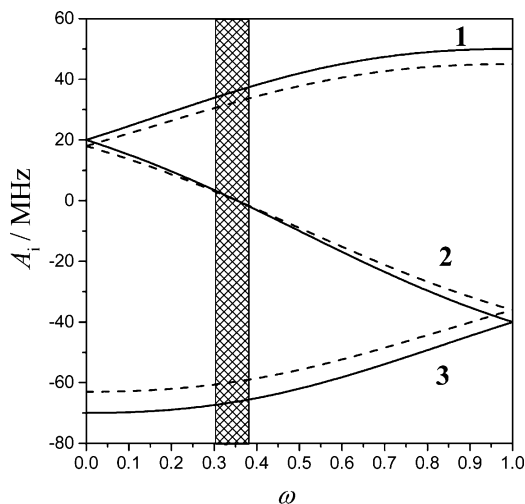
Figure 12. Dependence of $A_{iso,i}$ on the parameter ω. The solid lines are obtained for $a_i = -30$ MHz and the dashed lines for $a_i = -27$ MHz. The grid area indicates the range of values for parameter ω inferred from the $A_{iso,i}$ values quoted in Table 3.

implemented experimentally in the case of [3Fe−4S]$^+$ clusters.[12] Through the mixing of the pure S states, AE induces first an anisotropy on $\mathbf{A}_i$. We have calculated the induced anisotropy on the $\mathbf{A}_i$ values using a home-written program, which numerically diagonalizes eq 4, taking into consideration the manifolds with S up to $^5/_2$. From the EPR data presented above, an average value of ca. 3.0 cm^{-1} was deduced for the AE vector $|\mathbf{d}|$. For this value of $|\mathbf{d}|$, the anisotropies of $\mathbf{A}_i$, quoted in Table 3, can be predicted. We also find that the parameters $A_{iso,i} = (A_{x,i} + A_{y,i} + A_{z,i})/3$ are not significantly different from the (isotropic) values predicted in the absence of AE for a given set of J_{ij}'s. Moreover, any deviation from these values can hardly be discernible within the present experimental accuracy.[42]

In the context of the isotropic H_{HDvV} Hamiltonian, $A_{iso,i}$ depends on c_i, and this parameter depends on the relationship between the J_{ij} values[38a,39] and, more specifically, on the parameter ω:[12]

$$\omega = \frac{J_{12} - J_{13}}{J_{23} - J_{13}}, \quad \text{with } J_{23} > J_{12} > J_{13} \qquad (7)$$

In Figure 12, we plot the dependence of $A_{iso,i}$ on ω assuming two values for a_i, −27 and −30 MHz. It can be seen that the parameters $\mathbf{A}_i$ are very sensitive to J_{ij}'s. This sensitivity has the consequence that small distributions on J_{ij} induce severe distributions on $\mathbf{A}_i$, and this is reflected in the Mössbauer spectra as a broadening of the lines.[12,13] The existence of distributions on the exchange parameters was also evident from EPR spectroscopy.

From Figure 12, we find that the obtained $A_{iso,i}$ values fall in the range that corresponds to ω of ca. 0.33. Taking into

account the J-strain effects suggested by the EPR results, this value of ω should be considered as an effective average value over an unknown distribution.

The magnetic measurements presented above favor an isosceles triangle configuration. In this case, ω is either 0 ($J_{12} = J_{13} < J_{23}$) or 1 ($J_{12} = J_{23} > J_{13}$). We emphasize here that the Mössbauer spectra cannot be reproduced with $\omega = 0$ or 1.[43] We comment below on the apparent discrepancy between the magnetic measurements and the Mössbauer data. The magnetic susceptibility measurements reflect the bulk magnetic behavior of the sample. Hence, small distributions of J_{ij} values detected by other methods cannot be sensed through bulk magnetic measurements. For instance, if we assume that 50% of the clusters have a configuration favoring solution **a** and 50% favoring solution **b**, we will obtain equivalently acceptable fits to the experimental magnetic susceptibility data.

We observe from Table S1 in the Supporting Information that the average quadrupole splitting increases slightly for $T < 75$ K. This may reflect changes in the electronic states of, or structural rearrangements around, the ferric sites. In either case, the exchange integrals are expected to be also temperature-dependent. This temperature dependence of J_{ij} is expected to be small and hardly discernible in the magnetic susceptibility vs temperature measurements. However, a slight differentiation of the J_{ij} constants may be suggestive of a further reduction of the isosceles symmetry to a scalene one, justifying thus a value of ω different from 0 or 1. A scalene configuration for the ground state of triferric carboxylate-bridged clusters was also suggested by Takano from early Mössbauer experiments.[38a] Such lowering of the symmetry to a scalene configuration was also inferred from the analysis of liquid-helium-temperature INS data of some trinuclear chromium(III) complexes.[44]

Conclusions

Following the discovery of the interesting properties of the SMMs, the research toward the elucidation of the magnetic properties of polynuclear transition-metal complexes has been intensified during the last years. The study of oligonuclear clusters, such as clusters containing the {Fe$_3$O}$^{7+}$ core, is helpful in order to understand the role of certain factors in the modulation of these properties.

Complex **1** belongs to this class of compounds with the unique property that the iron sites are not equivalent because two iron sites possess a NO$_5$ coordination whereas for the third the coordination is O$_6$. This has the consequence that the 4-fold degeneracy of the ground state is lifted because of different exchange coupling constants. Hence, the ground state of the system is a well-isolated doublet. Magnetic susceptibility measurements have inherent limitations as a means for elucidating the characteristics of the magnetic exchange between paramagnetic ions with high accuracy. Thus,

(42) A second effect of AE is a "canting" of the individual spins with respect to the external magnetic field. This effect is of special importance in Mössbauer spectroscopy because the induced magnetic field on each nucleus is not parallel to the external magnetic field anymore, and this affects the transition probabilities for the transitions within the nuclear energy levels. These effects, however, cannot be resolved within the resolution of the present experimental spectra and do not affect the estimation of the $A_{iso,i}$'s.

(43) This is manifested by the fact that the analysis of the experimental spectra clearly demands the presence of an individual iron site for which $|A_{iso,i}|$ is small. From Figure 12, we can see that this can be achieved for ω of ca. 0.33.

(44) Jayasooriya, U. A.; Cannon, R. D.; White, R. W.; Stride, J. A.; Grinter, R.; Kearley, G. J. *J. Phys. Chem.* **1993**, *98*, 9303.

application of EPR and Mössbauer spectroscopies at liquid-helium temperatures revealed useful information regarding the nature of the magnetic interactions that would not have been accessible through magnetic measurements only.

From these studies, it is inferred that the isotropic HDvV Hamiltonian with a unique set of exchange coupling constants is not adequate to describe the magnetic properties of these clusters. Of importance also are (1) the presence of nonisotropic interactions and especially AE and (2) *J*-strain effects. Our analysis provides a quantitative determination for the contribution of these factors in the magnetic properties of these clusters.

Supporting Information Available: Crystallographic data in CIF format, Figure S1 showing the distributions of the $g_{\perp}$ values of the EPR spectra, and Table S1 noting Mössbauer parameters of the zero-field spectra. This material is available free of charge via the Internet at http://pubs.acs.org.

IC051652X